Journal of Systems Engineering and Electronics
Vol. 34, No. 4, August 2023, pp.924 – 938

# Modular flexible “Tetris” microsatellite platform based on sandwich assembly mode

ZHOU Jun [1,2,3], ZHANG Hao [1], LIU Guanghui [1,2,3,*], CHENG Cheng [1,2,3], and ZHANG Jiaolong

1. School of Astronautics, Northwestern Polytechnical University, Xi’an 710072, China;
2. National United Engineering Laboratory of Microsatellite Technology and Application, Xi’an 710072, China;
3. Shaanxi Engineering Laboratory for Microsatellites, Northwestern Polytechnical University, Xi’an 710072, China

**Abstract:** In this paper, a flexible modular “Tetris” microsatellite platform is studied to implement the rapid integration and assembly of microsatellites. The proposed microsatellite platform is fulfilled based on a sandwich assembly mode which consists of the isomorphic module structure and the standard mechanical-electric-data-thermal interfaces. The advantages of the sandwich assembly mode include flexible reconfiguration and efficient assembly. The prototype of the sandwich assembly mode is built for verifying the performance and the feasibility of the proposed mechanical-electric-data-thermal interfaces. Finally, an assembly case is accomplished to demonstrate the validity and advantages of the proposed “Tetris” microsatellite platform.

**Keywords:** modular microsatellite design, flexible platform, sandwich assembly mode, isomorphic module structure, standard mechanical-electric-data-thermal interface.

**DOI:** 10.23919/JSEE.2023.000094

## 1. Introduction

Motivated by the goal of “faster, better and cheaper”, the microsatellite technology has been developed [1−4] and is successfully applied in many fields such as earth observation, in-orbit services and deep space exploration [5−8]. In general, the microsatellite begins to design with a specific flight mission (such as in-orbit maintenance and space experiments), and the design process consists of mission proposal, requirement analysis, scheme design, fabrication, assembly, integration, testing and operation [9,10]. Based on the above process, the functions, sizes and dimensions of the satellites are restricted, which can only serve for a specific flight mission. With the increasing complexity of flight missions, especially in the case of emergencies such as earthquakes, floods and snowstorms, the flight missions are difficult to predict in advance, and the traditional satellite design methods cannot cope with such emergencies in time [11,12]. Consequently, novel microsatellite concepts and design methods that have the flexible reconfiguration ability is necessary to be investigated to achieve the rapid integration and operation of satellites, which can improve the efficiency in response to emergencies and complex flight missions [13,14].

Modular satellite is a new concept proposed in recent years, which is composed of modules with different functions [15] and aims for a cost-efficient reduction of the time to orbit [16]. Compared with the traditional satellite, the modular satellite can perform various flight missions by reconfiguring and updating the satellite systems [17]. Considering that the connection and cooperation among modules are complex, the modular and standard design technology becomes the key point to improving the design efficiency of a modular satellite. For example, a spacecraft named SMART-Bus is designed based on the modular design concept, providing a set of mechanical, electric and logical standards. SMART-Bus spacecraft consists of a stack of hexagonal modules, or “slices”, each of which performs a particular spacecraft subsystem function [18]. With the development of modular and standardized technology, the design complexity of the modules also needs to be considered. The Panel Extension

Manuscript received December 04, 2021.
*Corresponding author.
This work was supported by the National Natural Science Foundation of China (62103339; 62073261); Shaanxi Natural Science Basic Research Program (2023-JC-YB-569), and the Fundamental Research Funds for the Central Universities.

Satellite (PETSAT) proposed in [19] was made of several "functional panels" which were connected in a "plug-in" fashion and stowed into a small volume in one dimension. The latch mechanism was designed to connect panels. The electric interface provides 5 V (3 A) and 12 V (100 mA) bus, and the inter-integrated circuit (IIC) and controller area network (CAN) are used as the data bus. The thermal interface is used to homogenize temperature within panels and adopts capillary tube to transfer heat from one panel to another [20−22]. SPARC-X satellites are expanded in two dimensions by adding the same height blocks on a substrate. The blocks of SPARC-X are designed with standard power and data buses between them, and high-speed and low-speed interfaces are provided to accommodate different components [23]. The iBOSS project adopted a 40 cm×40 cm×40 cm cube structure as the standard module, and different subsystems and components can be integrated into the cubic modules [24,25]. The androgynous design allows the satellite to be efficiently assembled and expanded in three dimensions [26]. Regarding the iBOSS, the mechanical interface is driven by motors to provide the mechanical force to complete the mechanical interlock. The electric interface is switchable in both directions. The data interface provides CAN and Ethernet buses to achieve communication between modules [27]. The "Satlet" proposed by Phoenix is designed with standard structures to accommodate the relevant standard interfaces for payload on-orbit delivery systems. The docking mechanism designed for "Satlet" adopts a standard connector-pin as an independent coupling element to connect two adjacent cells [28,29].

Inspired by the building block model, a flexible modular "Tetris" microsatellite platform is proposed in this paper. In this work, standard modular configurations are designed to satisfy the assembly requirements of components. Standard interfaces can provide reliable mechanical, electric, data communication and thermal transfer paths. The modular microsatellite can be quickly assembled by connecting the modules. Based on this, the traditional satellite design process can be simplified into four steps: mission definition, satellite assembly, testing and operation. Compared with the existing modular microsatellites, the contributions of this paper are:

(i) A "sandwich" assembly mode (SAM) is proposed, which not only realizes the rapid assembly of modules in three dimensions but also generates a set of the standard assembly process to reduce the design cost and development time.

(ii) An improved symmetric "mechanical-electric-data-thermal" interface is proposed, which not only supports the assembly of modules at multiple angles but also improves the convenience and flexibility of satellite assembly.

(iii) Based on the SAM and standard design concept, the proposed modular microsatellite platform has rapid and flexible expansion capability and can be applied to a variety of application scenarios such as complex missions and emergencies.

The structure of this paper is as follows: Section 2 introduces an integrated SAM (iSAM) based flexible modular "Tetris" microsatellite platform. Section 3 introduces the isomorphic standard modules and interfaces for the iSAM. Section 4 verifies the performance and feasibility of the iSAM by simulations and experiments and demonstrates a modular assembly case of a 6U microsatellite platform prototype. Section 5 gives the conclusions.

## 2. Flexible modular "Tetris" microsatellite platform

In order to achieve rapid integration and assembly, the following principles should be considered in the design of a flexible modular "Tetris" microsatellite:

(i) Complete and independent functionality: Based on the complete functions, the structural coupling should be reduced to avoid repeated assembly and design.

(ii) Flexible assembly and rapid integration: To achieve flexible expansion, the constraints of satellite assembly topology and orientation should be reduced. The assembly process needs to be simplified to improve the efficiency of satellite integration.

(iii) Standardization and serialization: Standardized design can reduce the difficulty of assembly. Series design can reduce the cost and cycle of the satellite.

(iv) Adaptative to different missions: The function, structure and size of the satellite can be flexibly adapted to the requirements of the missions.

Based on the above design principles, a flexible modular microsatellite platform design scheme based on the iSAM is proposed, and the procedures for assembling a flexible modular "Tetris" microsatellite are shown in Fig. 1.

In the proposed scheme, different components are inte-

grated into the module in advance, so that modules become the basic unit of the satellite. The design of the standard interface not only provides reliable energy and signal transmission path but also enables a reliable connection between modules. Therefore, the traditional satellite design method can be converted into a module assembly process, which can avoid wasting time and costs caused by the repeated design.

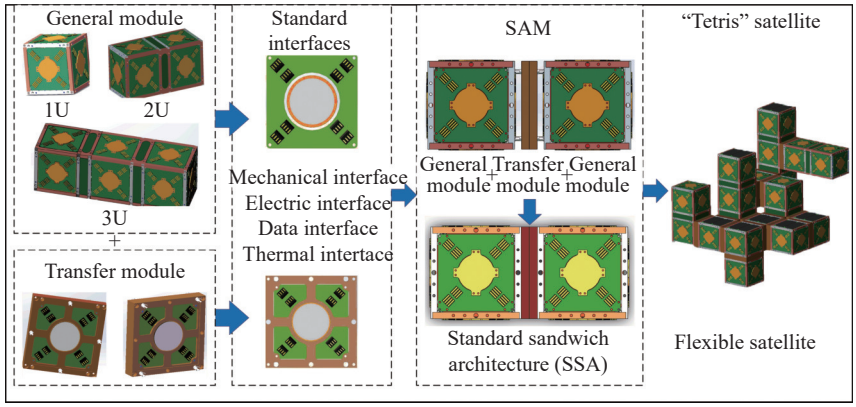


**Fig. 1 Procedures for assembling a flexible modular "Tetris" microsatellite**

In order to simplify the module assembly process, an iSAM (two general modules connected to one transfer module) is proposed, and the sandwich structure is schematically shown in Fig. 2. According to the iSAM, a satellite with any complex functions and shapes can be integrated and assembled by cascading or extending the sandwich structure. Even when encountering a complex and urgent mission, the satellite adapted to the new mission can be assembled only by adding or changing the modules of the sandwich structure.

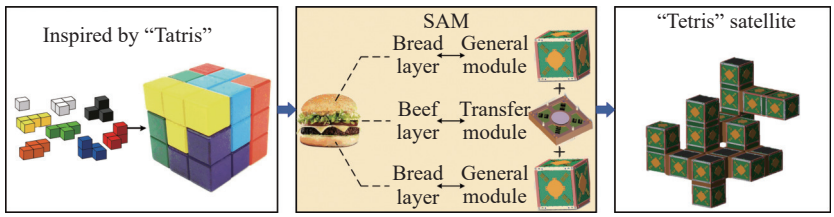


**Fig. 2 Concept design of flexible modular "Tetris" microsatellite**

## 3. Standard module and interface for iSAM

### 3.1 Modular structure design and integration

The design principles of modules are as follows:

(i) Functional independence and integrity: modules are independent in physical structure and have specific and complete functions.

(ii) Sufficient internal space: Sufficient space inside the modules should be provided for installing components.

(iii) Generalization and standardization: The generalized and standardized design enables the module to be compatible with existing components and avoid redesigning.

(iv) Serialized production: The module should support serialized production, which can reduce the cost and cycle.

The U-shaped structures are used to be the standard modules. To ensure functional integrity, components with independent functions are installed into U-shaped modules, which are defined as functional modules. In the iSAM, functional modules are used to assemble satellites, and the details are shown in Table 1. To reduce weight, the masses of the transfer module, the 1U\2U\3U general modules and the special module are 0.262 kg, 0.400 kg, 0.800 kg, 1.200 kg and 0.085 kg, respectively. In addition, a series of larger sizes and specifications of general modules (such as 4U, 6U, or even larger ones) can be implemented to adapt to larger sizes and shapes of components.

**Table 1 Details of standard 1U−3U general module structures and transfer module structure for iSAM**

| Type | Dimension | Function | Display |
|---|---|---|---|
| General module | 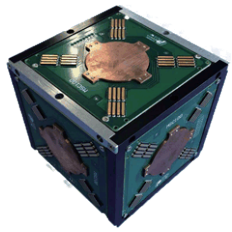 1U module (100 mm×100 mm×113.5 mm) | House-keeping | 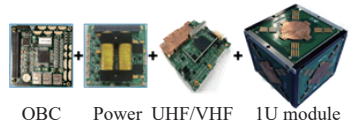 OBC Power UHF/VHF 1U module |
| | | GPS | 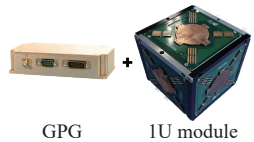 GPG 1U module |
| | | Data transmission | 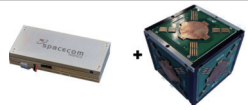 S/X-band transmitter 1U module |
| | 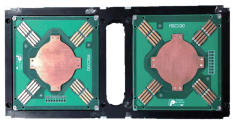 2U module (100 mm×100 mm×227 mm) | Power | 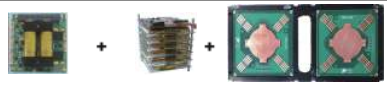 Power system Battery array 2U module |
| | | Sensor |  Sun sensor Star tracker Magnetometer 2U module |
| | | Control | 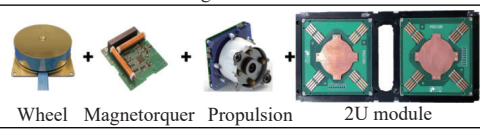 Wheel Magnetorquer Propulsion 2U module |
| | 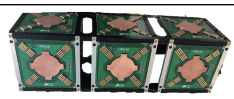 3U module (100 mm×100 mm×340.5 mm) | Payload | 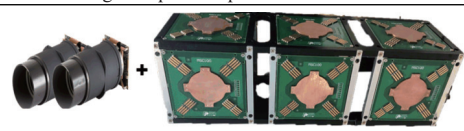 Cameras 3U module |
| Transfer module | 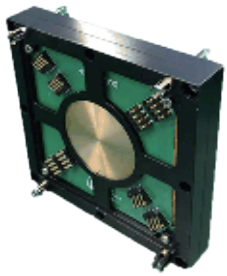 Sandwich structure (100 mm×100 mm×15.1 mm) | Connection | 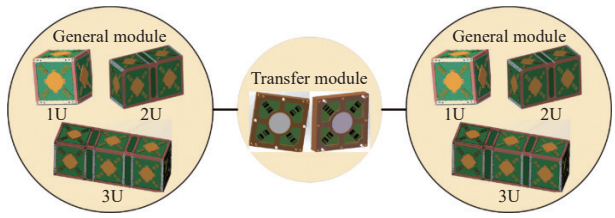  |
| Special module | 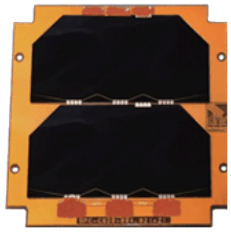 Solar panel (89 mm×98 mm×1.5 mm) | Power supply | 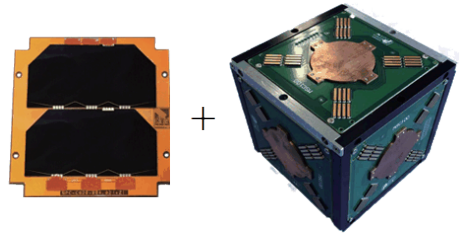 |

The functions of the modules depend on the integrated components. Combined with Table 1, different types of modules can be described as follows:

(i) The core module is integrated by an onboard com-

puter, a communication board and a power board, which can realize the basic functions of task scheduling, communication and power supply.

(ii) The GPS module consists of GPS receiver(s), which can be used to complete satellite positioning and clock synchronization.

(iii) The high-speed communication module consists of the S/X band transmitter, which can be used for high-speed data communication with large data volumes.

(iv) The power module is made up of batteries and an electrical power management unit, which can realize the expansion of electric energy.

(v) The sensor module is composited of sensors such as star sensors, gyroscopes and magnetometers, which are used for the acquisition of satellite attitude.

(vi) The control module consists of flywheels, magnetic moments and thrusters, etc., which can realize the attitude and orbit control of the satellite.

(vii) The payload module is composed of different payloads to accomplish specific missions.

(viii) The transfer module is used to connect with two general modules into the sandwich structure.

(ix) The solar cell module consists of standard solar cell panels, which are used to provide electric energy for the satellite system.

### 3.2 Mechanical-electric-data-thermal interface for iSAM

The design principles of the interfaces for the iSAM are as follows:

(i) The module interface should be versatile and can be applied to all general modules, transfer modules and special modules.

(ii) The interface has excellent performance and can provide a reliable energy-signal-mechanical connection path for the module.

(iii) The interface should be easy to connect, which can improve efficiency and reduce the constraints of the module assembly.

Based on the proposed principles, the isomorphic and standard mechanical-electric-data-thermal interface is designed as shown in Fig. 3.

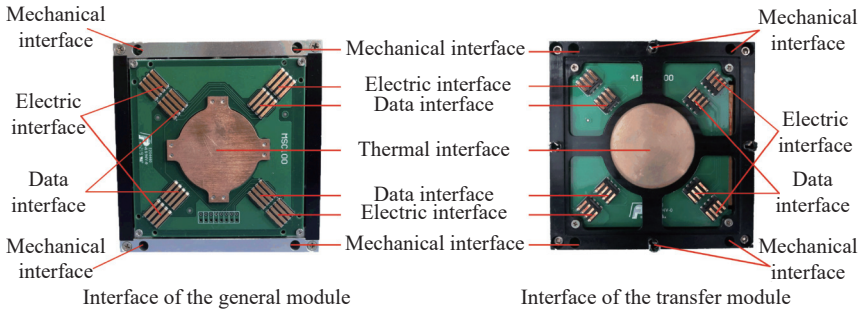


**Fig. 3 Standard "mechanical-electric-data-thermal" interface**

#### 3.2.1 Mechanical interface

The mechanical interfaces are designed as shown in Fig. 4, and the detailed scheme is as follows:

(i) Four groups of symmetrical mechanical interfaces are designed on the surface of the module, which can not only withstand mechanical stress but also support 90° rotational assembly.

(ii) To reduce the complexity, the mechanical interfaces of the general modules are designed as female interfaces, while the transfer modules and special modules are designed as male interfaces. Therefore, the sandwich structures have a uniform "female-male-female" interface connection mode.

(iii) The mechanical interface is designed by using the frame of the module so that the space inside the general module is not occupied and does not interfere with the installation of internal components.

(iv) The transfer module is designed with two types of mounting holes for mechanical interfaces. The mounting holes located at the corner of the frame support the assembly of the general module from the side, while the mechanical interface located at the center of the frame supports the assembly of the general module from the top and bottom. The advantage of this treatment is that it not only eliminates mechanical constraints caused by the assembly but also avoids duplicate designs and saves costs.

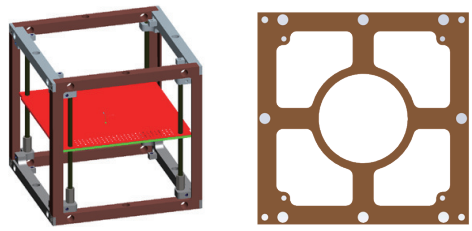

(a) Female interface of the general module (b) Female interface of the transfer module

**Fig. 4 Mechanical female interface of general module and transfer module**

Fig. 5 illustrates the structure of the mechanical male connector. The mechanical male connector adopts a specific structure that is made up of a cylindrical part with a barbed structure on the two ends. The cylindrical part in the middle of the male connector is used to support the transfer module, and the barbed structure on the two ends is used to connect with the general module. The advantage of the male connector is that the docking process (such as the lock and release for the general modules) can be reached easily, and the orbital load can be transferred and sustained. By manual insertion and removal, the general module can be easily re-assembled.

**Fig. 5 Mechanical male connector**

### 3.2.2 Electric and data interface

The electric interface and the data interface are designed as shown in Fig. 3, which have the same distribution form. The details of the interface scheme are as follows:

(i) The electric interfaces and data interfaces are designed as the surfaces contacted interface. To follow the "female-male-female" pattern, the female interfaces are mounted on the general modules and the male interfaces are mounted on the transfer modules and special modules.

(ii) The insulated bases of the female and male interfaces are soldered to the printed circuit boards (PCBs) of the general module and the transfer module, respectively. Special cables are designed inside the general module to connect with four groups of contacts on the insulated base so that a reliable transmission path of energy and signals can be established.

(iii) Considering the performance requirements, the same four groups of electric interfaces and four groups of data interfaces are designed on the surface of the module, which is all distributed diagonally. Thus, the module can be assembled with a 90° option.

(iv) The electric interface is designed with a 5 V and 12 V dual power bus. To provide enough power, the power design requirements of the electric interface are shown in Table 2.

**Table 2 Power design requirements of the electric interface**

| Interface | Quantity | Current of each group interface/A | Power of each group interface/W | Maximum power/W |
|---|---|---|---|---|
| 5 V | 4 | 3 | 15 | 60 |
| 12 V | 4 | 3 | 36 | 144 |

(v) The data interface is designed with a dual data bus of CAN and USB. In addition, the standard CAN open protocol and USB protocol are used for the corresponding data buses respectively, thus allowing a series of complex operations such as device identification, driver management, parameter reconfiguration and task scheduling.

Based on the physical interface, hardware bus and software protocol, a plug-and-play network of satellite systems can be constructed as shown in Fig. 6. Components and modules can be connected to the satellite system and can be autonomously identified and configured through the plug-and-play network.

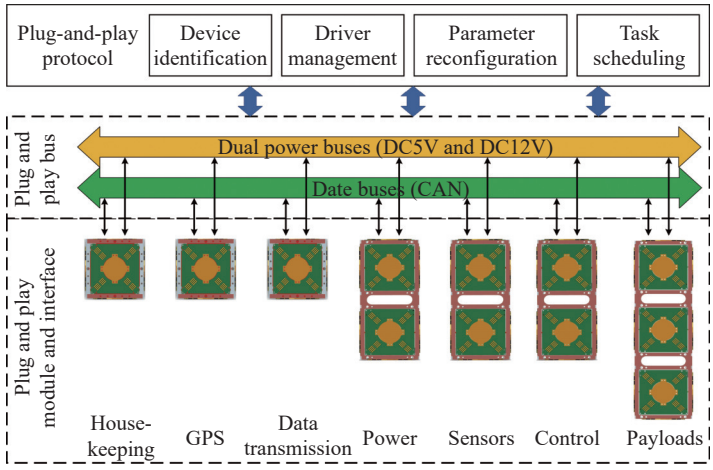


**Fig. 6 Architecture of plug-and-play system based on the electric and data interface**

To manage the electric and data loops between modules, a module management unit (MMU) is designed as shown in Fig. 7.

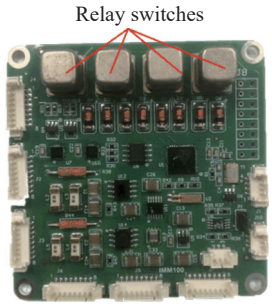


**Fig. 7 Module management unit**

The MMU consists of an intelligent microprocessor, two Hall current sensors and four groups of relay switches.

For the electric interface, the Hall current sensor monitors the current value of the interface in real-time and the intelligent processor samples it to determine the status of the power circuit. Once an overcurrent fault occurs, the intelligent processor will control the relay to cut off the electric interface, so that the back-end devices can be protected.

For the data interface, if the intelligent processor cannot interact with the onboard computer, the data interface will be cut-off by the relay. The processing actions of the module management unit are shown in Fig. 8.

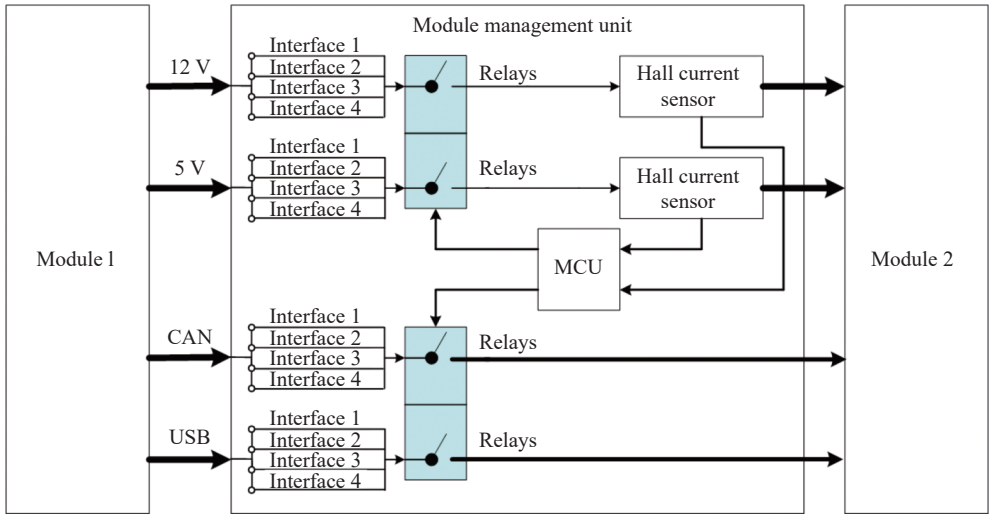


**Fig. 8 Processing actions of MMU**

To ensure that the electric and data communication of the module management unit can have high reliability, the power (5 V and 12 V) and data (CAN and USB) interfaces are connected to the relay switches in a 4-point redundant way, and the output of the relay is connected to the module management unit. In addition, the module management unit can effectively avoid star or ring connections of the data bus by controlling the connection of the data interfaces.

### 3.2.3 Thermal interface

The distribution of the thermal interfaces is shown in Fig. 3. The function of the thermal interface is to provide a reliable heat transfer path between the modules so that the heat generated by the modules can be transferred to adjacent modules and eventually released into outer space. As a result, the temperature inside the module can be maintained within a healthy range. The schemes of the thermal interface are as follows:

(i) The thermal interface adopts the face contact interface pattern, which consists of a female interface and a male contact block. The female interface is mounted on the general module using a flange with four groups of threaded holes, while the male contact block is a hollowed-out brass cylinder embedded in the transfer module. The structure of the thermal interface is shown in Fig. 9.

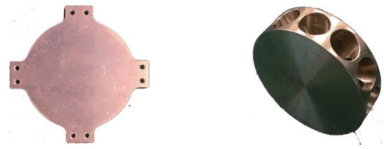

(a) Female contact sheet (b) Male contact block

**Fig. 9 Female contact sheet and male contact block**

(ii) The thermal interface is located in the center of the module and is symmetrical so that it can be assembled by rotating 90°.

(iii) To provide an efficient heat transfer path, the thermal interface between the general module and the transfer module has a high thermal conductivity. The parameters of the thermal interface are shown in Table 3.

**Table 3 Parameters of female contact sheet and male contact block**

| Type | Material | Shape | Diameter/mm | Thickness/mm | Thermal conductivity/ (W/(m·K)) | Specific heat capacity/ (J/(kg·K)) |
|---|---|---|---|---|---|---|
| Female contact sheet | Copper | Round sheet with flange | 40 | 1.4 | 401 | 385 |
| Male contact block | Brass | Hollowed-out cylinder | 45 | 13 | 110 | 380 |

Fig. 10 illustrates the heat transfer process.

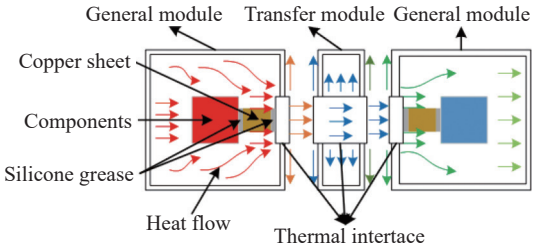


**Fig. 10 Heat transfer process**

The copper plate is used as the heat transfer medium between the thermal interface and the internal components of the module. One side of the copper plate is connected to the heat-generating surface of the component and the other side is connected to the inner surface of the thermal interface. To avoid contact thermal resistance at the connection site, silicone grease is applied uniformly to the surface of the copper plate to ensure adequate contact. According to this strategy, the heat generated by the component can be transferred through the silicone grease-copper plate-thermal interface pathway and eventually to the adjacent modules.

## 4. Simulations and experiments

In this section, the performance of the standard interface for the proposed iSAM is validated. An assembly example is implemented to verify the feasibility of the proposed flexible modular "Tetris" microsatellite platform and is compared with the state-of-the-art modular satellite schemes.

### 4.1 Verification of the mechanical-electric-data-thermal interface for iSAM

Experiments are designed to verify the feasibility and performance of the mechanical-electric-data-thermal interface for the iSAM. To visualize the experimental protocol, the experimental method and devices are presented as shown in Table 4.

**Table 4 Experiment conditions of the interfaces**

| Interface to be tested | Experimental basis | Experimental device |
|---|---|---|
| Mechanical interface | Tensile strength | Tension tester with a range of 0−500 kg and an accuracy of 1% |
| | | A testing computer |
| Electric interface | Ohm's law and power principle | An ohmmeter with a measurement range of 0−200 and an accuracy of ±0.05% of the reading |
| | | Dual-channel digital power with 0−30 V DC voltage and 0−3.5 A current |
| | | A 4-channel oscilloscope with a sampling rate of 1 GS/s |
| | | A 10 (150 W) sliding resistor |
| Data interface | Signal attenuation and distortion | A signal generator |
| | | A 4-channel oscilloscope with a sampling rate of 1 GS/s |
| Thermal interface | Fourier's law and Joule's law | A film heater |
| | | A dual-channel digital power that can provide two 12 Vvoltages |
| | | The temperature sensor (PT100) |
| | | A 4-channel temperature transmitter |
| | | A thermostat |
| | | A testing computer |

#### 4.1.1 Feasibility verification of mechanical interface

The barbed structure is subjected to mechanical deformation due to the pressure as it passes through the mechanical interface. The pressure, shear force and torque of the barbed structure are mechanically limited by the mechanical interface, and the tensile force of the general module and the transfer module is determined by the cross-sectional shape of the barbed structure. In the process of insertion and removal, the deformations of the barbed structure can be calculated in the following equations:

$$\sigma_{\max} = \frac{F_p a}{bd^2/6}, \tag{1}$$

$$\mathrm{df} = \frac{F_p a^3}{3EI} = \frac{\sigma_{\max}}{E} \cdot \frac{2a^2}{3d}, \tag{2}$$

where $F_p$ is the force applied to the lateral of barbed structure, $a$ is the length; $b$ is the width, $d$ is the thickness, $\sigma_{\max}$ is the maximum bending stress, $E$ is elastic modulus, $I$ is the moment of the area, and df is deformation at the ends.

In order to verify the feasibility of the mechanical

interface, the simulation for the deformations of the barbed structure is accomplished by using the workbench 19.0 simulation platform.

The mesh conditions of the mechanical interface are set as follows:

(i) The mesh method for the mechanical interface adopts the hex dominant.

(ii) The element size of the mechanical interface is 0.3 mm.

The simulation conditions of the mechanical interface are set as follows:

(i) The material of the mechanical interface is aluminum alloy, and the density is 2 770 kg/m$^3$. The Young's modulus is $7.2\times10^{10}$ Pa, and the Poisson's ratio is 0.33.

(ii) The pressure on the barbed structure increases from 0 to 3.5 N linearly.

(iii) The simulation time is set to 1 s.

Based on the above conditions, the deformation of the bared structure is shown in Fig. 11, and the maximum deformation of each barbed structure is 1.23 mm.

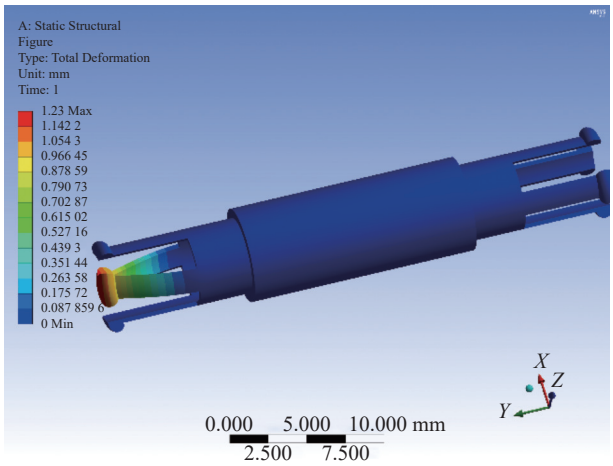


**Fig. 11 Deformation of mechanical interface**

In order to measure the maximum tensile force, a tension tester is used as the testing device for the mechanical male connector. The tension tester has a testing range of 0−500 kg with a measurement accuracy of 1%.

The experimental principle is as follows: the load sensor is installed on the fixture when the tester begins to work, and the load sensor obtains the tension value. After amplifying the tension signal through A/D for data acquisition and conversion, transmit the data to the computer for recording.

The experimental method is as follows: the mechanical male connectors are fixed on both ends of the tension tester, and the tension tester gradually increases the tensile force from 0 N until the mechanical mechanism is pulled off. Five mechanical male connectors (ignoring the manufacturing process error) are tested and the average value is calculated. Based on the method, the results are shown in Table 5.

**Table 5 Strength of mechanical interface**

| Mechanical interface | Tension force/N |
|---|---|
| 1 | 999.89 |
| 2 | 1 000.35 |
| 3 | 1 000.06 |
| 4 | 1 000.13 |
| 5 | 999.86 |
| Average value | 1000.06 |

According to the experiment, the mechanical male connector can withstand an average pulling force of 1 000.06 N. Therefore, it is considered sufficient to cope with loads on the orbit, such as gravity gradient, aerodynamics, orbital disturbances, and system attitude control, orbital control overloads.

### 4.1.2 Feasibility verification of electric and data interface

The contact state of the electric and data interface determines the efficiency of signal and energy transmission. In order to verify the feasibility, the contact state, power conduction capability and signal transmission capability of the interface need to be demonstrated.

(i) Verification of the contact state of the electric and data interfaces

The principle of the designed experiment is as follows: the resistance of the contact surface is measured to determine the degree of energy loss as it passes through the interface. An ohmmeter with a measurement range of 0−200 Ωm and an accuracy of ±0.05% of the reading is used as the experimental device to measure the resistance of the interface. The experiment platform is shown in Fig. 12.

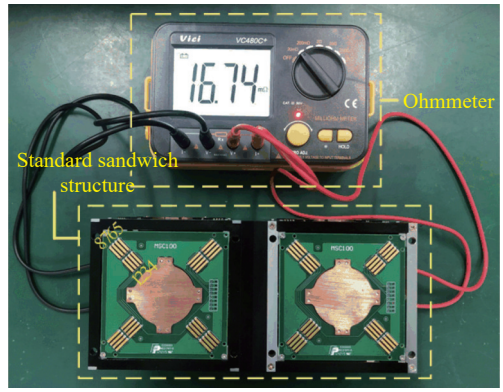


**Fig. 12 Experiment platform of the contact state for the electric and data interface**

The experimental method is as follows: Testing cables are welded to facilitate the measurement by the ohmmeter. The resistance values between every two corresponding cables are measured. Since the resistance of the cables cannot be ignored, the resistance values of all cables have been obtained in advance. Therefore, the resistances of the interfaces are the difference values between the total resistance and the resistance of the two cables. It can be expressed by the following equation:

$$R_{ir} = R_t - R_{cr} \tag{3}$$

where $R_t$ is the total resistance between the cables on the two ends, $R_{cr}$ is the sum resistance of cables, and $R_{ir}$ is the interface resistance.

In order to reduce the error, the resistance of cables and the total resistance is measured 20 times, and the average value is calculated to be the interface resistance.

Table 6 illustrates the cable resistance, total resistance, and interface resistance, respectively.

**Table 6 Resistance value** mΩ

| Interface | Cable resistance | Total resistance | Interface resistance |
|---|---|---|---|
| 1 | 6.99 | 16.74 | 9.75 |
| 2 | 7.61 | 18.16 | 10.55 |
| 3 | 6.93 | 17.40 | 10.47 |
| 4 | 6.61 | 17.30 | 10.69 |
| 5 | 6.65 | 16.86 | 10.21 |
| 6 | 6.99 | 17.25 | 10.26 |
| 7 | 7.08 | 18.30 | 11.22 |
| 8 | 7.11 | 17.34 | 10.23 |

The experimental results show that the maximum total resistance is 18.30 mΩ, after subtracting the cable resistance on two sides of the general module, the maximum resistance of interface resistance is 11.22 mΩ, while the minimum is 9.75 mΩ. Considering the standard sandwich architecture is composed of two general modules and one transfer module, the interface resistance is a sum of two contact resistances. It can be indicated that the contact resistance between the electric and data interface is too small to impact the transmission of the electric signals.

(ii) Verification of the power conductive capability of the electric interface

The power conduction capability of the electric interface depends on the voltage and current that can be provided by the interface contacts. Based on Ohm's law and power calculation principles, the experimental platform shown in Fig. 13 is designed to verify the power conduction capability. In the experiment, dual-channel digital power with 0−30 V DC voltage and 0−3.5 A current is used as the power device. A 4-channel oscilloscope with a sampling rate of 1 GS/s is used to measure the voltage and a multimeter with a resolution of 0.1 μA is used to measure the current. The test load for the experiments is a 10 Ω (150 W) sliding resistor.

(a) 5 V interface experiment platform (b) 12 V interface experiment platform

**Fig. 13 Experiment platform for 5 V and 12 V electric interfaces**

The experimental method is as follows: For the sandwich structure, the dual-channel digital power is connected to the 5 V and 12 V interfaces, and the test load is connected to the interface. The power of the electric interface is calculated by adjusting the voltage and current values of the digital power, which can be expressed as

$$P_{tl} = U_{tl} I_c \tag{4}$$

where $U_{tl}$ is the voltage of the test load. $I_c$ is the current of the circuit. $P_{tl}$ is the power of the test load.

According to the experimental results shown in Fig. 14, the voltage of the 5 V interfaces and 12 V interfaces are 5.49 V and 12.5 V, and the currents are 3.098 A and 3.129 A. Therefore, the electric interface can provide more than 3.0 A, which can satisfy the requirements.

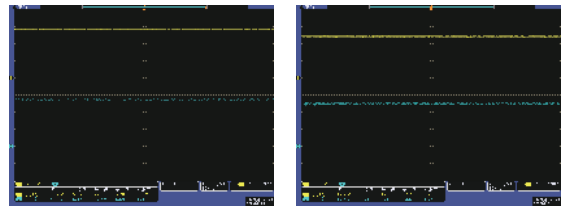

(a) Voltage of the 5 V electric interface (b) Voltage of the 12 V electric interface

**Fig. 14 Voltage of 5 V and 12 V electric interfaces**

(iii) Verification of the signal transmission capability of the data interface

The square wave signals of different frequencies are used to simulate the information transmitted by the data interface, and the performance of the data interface is judged by testing the attenuation and distortion of the signals on both sides of the interface. The experimental platform is constructed as shown in Fig. 15.

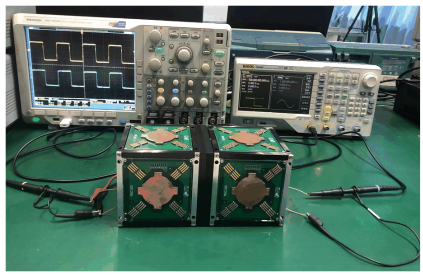

**Fig. 15 Experiment platform of data interface**

The experimental principle and method are set as follows: the signal generator is used to generate four groups of square wave signals with an amplitude of 10 V, a duty cycle of 50%, and frequencies of 200 kHz, 500 kHz, 1 MHz and 2 MHz to simulate the data transmission process of CAN bus with different baud rates. A 4-channel oscilloscope is used to observe the waveforms on both sides of the data interface, and waveforms are as shown in Fig. 16. By comparing the signal of the signal generator (input signal) with the signal of the data interface (output signal), comparison results are shown in Table 7.

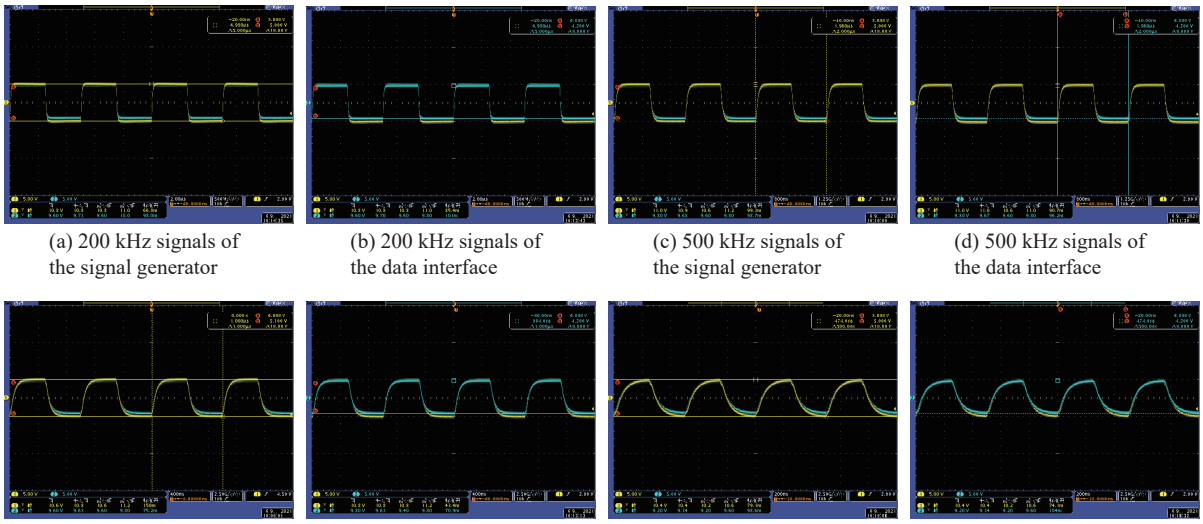

(a) 200 kHz signals of the signal generator

(b) 200 kHz signals of the data interface

(c) 500 kHz signals of the signal generator

(d) 500 kHz signals of the data interface

(e) 1 MHz signals of the signal generator

(f) 1 MHz signals of the data interface

(g) 2 MHz signals of the signal generator

(h) 2 MHz signals of the data interface

**Fig. 16 Signals of the signal generator and the data interface**

**Table 7 Comparison results of signals in different frequencies**

| Frequency | Signal of the signal generator | | Signal of data interface | | Comparison | |
|---|---|---|---|---|---|---|
| | Amplitude/V | Duty ratio/% | Amplitude/V | Duty ratio/% | Amplitude attenuation/V | Phase delay |
| 200 kHz | 10.8 | 50 | 9.6 | 50 | 1.2 | 0 |
| 500 kHz | 11.0 | 50 | 9.8 | 50 | 1.2 | 0 |
| 1 MHz | 10.8 | 50 | 9.8 | 50 | 1.0 | 0 |
| 2 MHz | 10.4 | 50 | 9.2 | 50 | 1.2 | 0 |

According to Fig. 16 and Table 7, with the frequency of the input signal increasing, the frequency of the output signal also increases.

Influenced by the signal generator, when the frequency reaches 1 MHz, the signal of the generator has already undergone significant distortion. When the signal frequency reaches 2 MHz, the rise time and fall time reach 120 ns and 180 ns respectively. Even so, the output signal still follows the input signal without phase delay. It can be shown that the output signal can follow the input signal. Due to the internal resistance of the data interface and the transmission line, the amplitude of the output signal is lower than the input signal, but it has little effect on the data transmission. Therefore, the data interface is designed for reliable data transmission within 2 MHz, which can be adapted to the CANopen protocol.

#### 4.1.3 Feasibility verification of thermal interface

In order to test the heat transfer capability of the thermal interface, the heat transfer process of the thermal interface is analyzed. The combined characteristics of heat conduction, heat convection and heat radiation are fully considered, and an experimental platform is built as shown in Fig. 17.

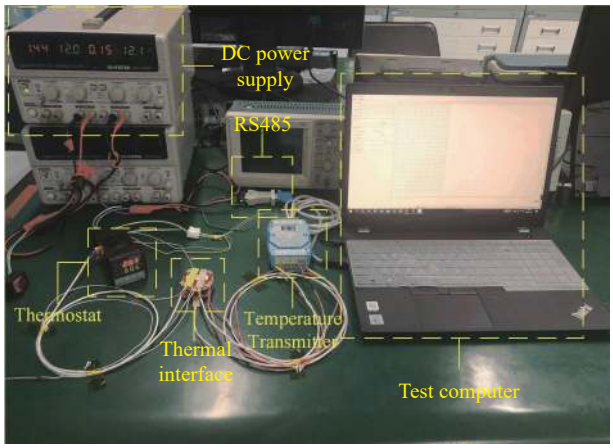


**Fig. 17 Experiment platform of the thermal interface**

The circular thin-film heater is a fully covered resistive network with the following parameters: 40 mm diameters, 0.2 mm thickness and 20 W power. A dual-channel digital power is used to provide two 12 V voltages. According to Fourier's law and Joule's law, the energy output from the heater can be converted into thermal energy, which increases the temperature of the heater. The temperature sensor (PT100) is the temperature measurement device. In addition, a 4-channel temperature transmitter is used to obtain the temperature information.

Based on the above experimental principles as well as the devices, the experimental method is as follows: the film heater is attached to the upper surface of the parent contact piece to provide heat to the thermal interface. Three temperature sensors (PT100) are used to measure the temperature of the thermal interface, as shown in Fig. 18. The first two temperature sensors are connected to the heat-generating surface and the measuring surface, and the third temperature sensor is connected to a thermostat to control the temperature of the film heater in real-time. All three temperature sensors are calibrated so that the initial temperatures of these sensors are the same. When the thin film heater is operating, the resistance values of the temperature sensors are converted into temperature information by a 4-channel temperature transmitter, and the temperature information is transmitted to the test computer via the RS485 bus at a baud rate of 57 600 bit/s and a transmission period of 1 s.

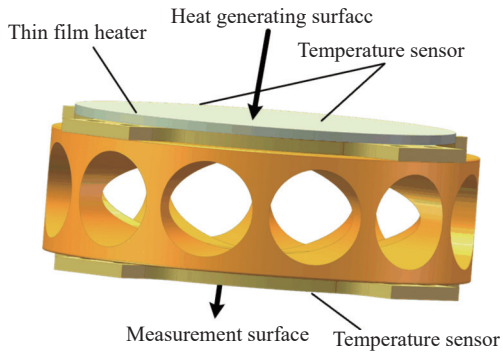


**Fig. 18 Details of the thermal interface**

Both the ambient temperature and the thermal interface temperature are 26.7 ℃, and the temperature of the heat-generating surface is controlled by the thermostat to keep it at 60 ℃. The measurement time is 485 s.

As shown in Fig. 19, the temperature of the measurement surface increases from 26.7 ℃ to 52.3 ℃ in 485 s. As the temperature difference becomes smaller, the heat flow becomes smaller as well. Due to the ability to raise the high temperatures in a short time, the designed thermal interface has a good heat transfer capability.

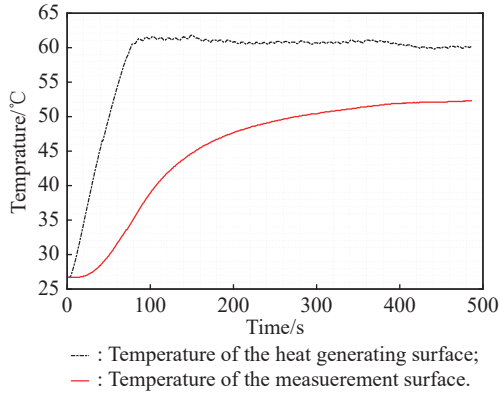


**Fig. 19 Temperature of the thermal interface**

### 4.2 A modular assembly case of the 6U prototype based on iSAM

An assembly case is used to verify the feasibility of the flexible modular "Tetris" microsatellite assembly mode including two 1U general modules and one transfer module as shown in Fig. 20, and the 3-dimensions expansion of the general module in the form of the iSAM is shown in Fig. 21.

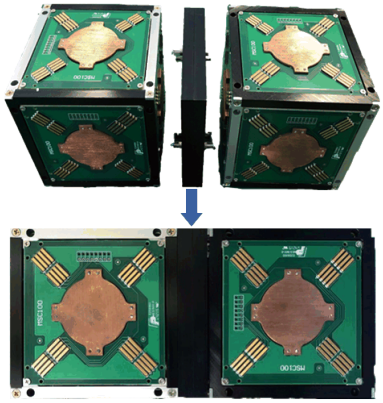

Fig. 20 SAM

Fig. 21 Modular assembly in 3-dimensions

Considering the mechanical characteristics of the modules, the expansion of modules, and the connection of interfaces between modules, the above characteristics can be well represented by assembling the 1U/2U/3U modules into a 6U microsatellite. Therefore, the assembly case of a 6U microsatellite is used as a validation example, and the conceptual design and implementation of assembling a 6U microsatellite are illustrated in Fig. 22 and Fig. 23, respectively.

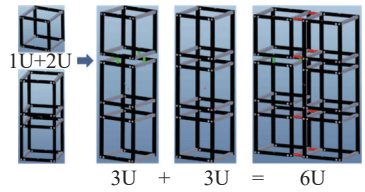


Fig. 22 Concept design of flexible assembly of a 6U microsatellite

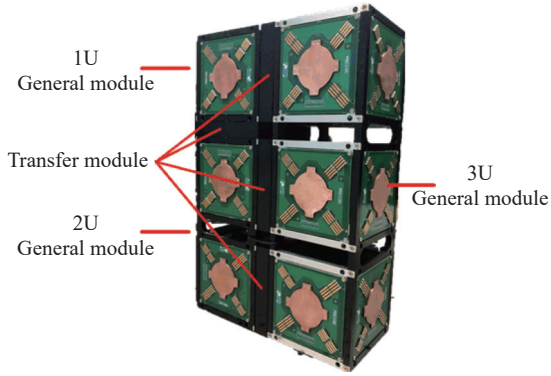


Fig. 23 Implementation or flexible assembly of a 6U microsatellite

A series of factors such as the flexibility of assembly, the design complexity and cost are necessary to be considered. To reflect the advantages of the proposed microsatellite platform, the comparison between the proposed modular microsatellite and the state-of-the-art modular microsatellite schemes is accomplished as shown in Table 8.

Table 8 Comparison of different modular microsatellite schemes

| Modular satellite | Module structure | Dimension that supports assemble | Specification and shape of the microsatellite |
|---|---|---|---|
| PETSAT [21−23] | Panel | 1 | − |
| SPARC-X [24] | Cube | 2 | Limited |
| iBOSS [25,26] | Cube | 3 | Any specifications and shapes |
| Tetris | Cube | 3 | Any specifications and shapes |

The advantages of the proposed flexible modular "Tetris" satellite have been verified. The adoption of the standard cube structure allows for 3-dimensional expansion of the general modules. The special surface contact interface makes that there is adequate space for integrating components. Consequently, the proposed modular satellite can be applied to different missions, and a new modular microsatellite with any specifications and shapes can be flexible and rapidly assembled by replacing the general modules.

## 5. Conclusions

The feasibility and advantages of a modular microsatellite platform based on a sandwich assembly mode are demonstrated in this paper. The proposed modular satellite platform can be extended in three dimensions. The standard module configuration and interfaces provide excellent performance and do not hinder the integration of components inside the module. In addition, the solar panels are designed with standard mechanical-electric-thermal-data interfaces that are well compatible with the

module’s interfaces. Therefore, the solar panels will work after assembling the solar panels to modules. Based on the proposed satellite platform and assembly scheme, flexible microsatellites of any size can be assembled efficiently and rapidly, which shows their ability to adapt to different missions.

In the future work, the plug-and-play and self-reconfigurable standard software architecture for flexible modular microsatellites will be further investigated to improve the extension and reconfiguration ability of the onboard software, so that the corresponding device drivers, parameter configurations and task scheduling sequences can be rapidly constructed and be prepared to use when a new functional module is assembled. With reduced software configuration and reconfiguration time, the flexible modular microsatellites based on a standardized onboard software architecture will have faster mission response capability to adapt to the diverse flight missions.

## References


[1] MARIA A V, NICOLE V, SABRINA C, et al. Interplanetary CubeSats system for space weather evaluations and technology demonstration. Acta Astronautica, 2014, 104(2): 516–525.

[2] ADDAIM A, KHERRAS A, ZANTOU E B. DSP implementation of integrated store-and-forward APRS payload and OBDH subsystems for low-cost small satellite. Aerospace Science and Technology, 2008, 12(4): 308–317.

[3] GAUDENZI P, ATEK S, CARDINI V, et al. Revisiting the configuration of small satellites structures in the framework of 3D additive manufacturing. Acta Astronautica, 2018, 146: 249–258.

[4] KOPACZ J R, HERSCHITZ R, RONEY J. Small satellites an overview and assessment. Acta Astronautica, 2020, 170: 93–105.

[5] WU S F, ZHAO T C, GAO Y, et al. Design and implementation of a cube satellite mission for antarctic glacier and sea ice observation. Acta Astronautica, 2017, 139: 313–320.

[6] YU X Z, ZHOU J, ZHU P J, et al. Star of AOXiang: an innovative 12U CubeSat to demonstrate polarized light navigation and microgravity measurement. Acta Astronautica, 2018, 147: 97–106.

[7] PALLICHADATH V, TURMAINE L, MELAIKA A, et al. In-orbit micro-propulsion demonstrator for pico-satellite applications. Acta Astronautica, 2019, 165: 414–423.

[8] HUANG P F, WANG M, MENG Z J, et al. Attitude takeover control for post-capture of target spacecraft using space robot. Aerospace Science and Technology, 2016, 51: 171–180.

[9] NIETO P C, EMAMI M R. CubeSat mission: from design to operation. Applied Science, 2019, 9(15): 3110.

[10] ESHAQ M, IBRAHIM A M, EISAAL S, et al. Information processing and digital communications in a modular satellite. Proc. of the 4th International Conference on Signal Processing and Information Security, 2021: 72−75.

[11] CAO X B. Flexible platform based micro-satellite design method. Aerospace Science and Technology, 2016, 53: 162–168.

[12] SYED M A, MUHAMMAD S B. Modular & COTS based power system for small LEO satellite. Proc. of the International Conference on Aerospace Science & Engineering, 2013: 1−3.

[13] SONG Q L, YE D, SUN Z W, et al. Autonomous reconfiguration of homogeneous pivoting cube modular satellite by deep reinforcement learning. Proc. of the Institution of Mechanical Engineers. Part I: Journal of Systems and Control Engineering, 2021, 235(10): 1777–1786.

[14] OSTERLOH T, DAHMEN U, ROBMANN J. Full lifecycle support for modular satellite systems provided by comprehensive virtual testbeds. Proc. of the International Symposium on Artificial Intelligence, Robotics and Automation in Space, 2018: 1−8.

[15] RIZWAN M M, ANWAR A, LEONARDO M R. Plug-and-play design approach to smart harness for modular small satellites. Acta Astronautica, 2014, 94(2): 754–764.

[16] OSTERLOH T, ROSSMANN J. A rigid body dynamics simulation framework for the analysis of attitude control systems of modular satellite systems. Proc. of the IEEE International Systems Conference, 2019: 1−8.

[17] HUANG P F, CHANG H T, LU Z Y, et al. Key techniques of on-orbit service-oriented reconfigurable cellularized satellite and its prospects. Journal of Astronautics, 2016, 36(1): 1–10.

[18] MCDERMOTT S. Aeroastro’s smart-bus: a low-cost modular approach enabling responsive space missions. Proc. of the AIAA 3rd Responsive Space Conference, 2005: 20–26.

[19] NAKASUKA S, SAHARA H, SUGAWARA Y, et al. A novel satellite concept “Panel Extension Satellite (PETSAT)” consisting of plug-in, modular, functional panels. Proc. of the 21st Annual AIAA/USU Conference on Small Satellites, 2007. https://digitalcommons.usu.edu/smallsat/2007/all2007/37/.

[20] YOSHIKI S, HIRONORI S, SHINICHI N, et al. A satellite for demonstration of panel extension satellite (PETSAT). Acta Astronautica, 2008, 63(1/4): 228–237.

[21] SHINICHI N, YOSHIKI S, HIRONORI S, et al. System design and control aspect of a novel satellite concept “panel extension satellite (PETSAT). Proc. of the 17th IFAC World Congress, 2008: 6−11.

[22] YOSHIKI S, SHINICHI N, KENJI H, et al. Structure and thermal control of panel extension satellite (PETSAT). Acta Astronautica, 2009, 65(7/8): 958–966.

[23] JAMES L, KYLE Z, EVA B, et al. SPARC-1: a joint US/Sweden multi-mission modular nanosatellite platform. Proc. of the IEEE Aerospace Conference, 2016: 1−16.

[24] KORTMANN M, SCHERVAN T, SCHMIDT H, et al. Building block–based “iBOSS” approach: fully modular systems with standard interface to enhance future satellites. Proc. of the 66th International Astronautical Congress, 2015: 1−11.

[25] JANSEN F, BRANDT T, DAFNIS A, et al. INPPS flagship with iBOSS building blocks. Proc. of the International Astronautical Congress, 2019. https://elib.dlr.de/134395/.

[26] KORTMANN M, MEINERT T, SCHRODER K, et al. Design and qualification of a multifunctional interface for modular satellite systems. Proc. of the 69th International Astronautical Congress, 2018: 1−5.

[27] SCHERVANA T A, KREISELB J, SCHROEDERC D, et al. New horizons for exploration via flexible concepts based on

building blocks using the standardized ISSI (intelligent space system interface) modular coupling kit by iBOSS. Proc. of the Global Space Exploration Conference, 2021: 14−18.

[28] BARNHART D, SULLIVAN B, HUNTER R, et al. Phoenix program status - 2013. Proc. of the AIAA SPACE Conference and Exposition, 2013: 5341.

[29] SULLIVAN B, BARNHART D, HILL L, et al. DARPA Phoenix payload orbital delivery system (PODs): "FedEx to GEO". Proc. of the AIAA SPACE Conference and Exposition, 2013: 5484.

## Biographies

**ZHOU Jun** was born in 1966. He received his B.S., M.S., and Ph.D. degrees from Northwestern Polytechnical University in 1988, 1990 and 1993, respectively. Currently, he is a professor at the School of Astronautics, Northwestern Polytechnical University. His research interests include satellite, system engineering, guidance, navigation and control.

E-mail: zhoujun@nwpu.edu.cn

**ZHANG Hao** was born in 1992. He received his B.S. and M.S. degrees from Xi'an Polytechnic University in 2014 and 2017, respectively. He is currently working toward his Ph.D. degree at the School of Astronautics, Northwestern Polytechnical University. His research interests are satellite engineering, system design and optimization.

E-mail: aiwuzh2016@163.com

**LIU Guanghui** was born in 1983. He received his B.S., M.S., and Ph.D. degrees from Northwestern Polytechnical University in 2006, 2009 and 2012, respectively. Currently, he is an associate researcher at the School of Astronautics, Northwestern Polytechnical University. His research interests include satellite system engineering and experimental design and evaluation.

E-mail: liuguanghui@nwpu.edu.cn

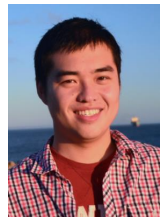

**CHENG Cheng** was born in 1986. He received his B.S. and M.S. degrees from Northwestern Polytechnical University, Xi'an, China, in 2008 and 2011, and Ph.D. degree from University of Toulouse, France, in 2015. He is currently an assistant professor with the School of Astronautics, Northwestern Polytechnical University. His research interests are statistical signal processing, estimation and detection theory, Bayesian inference and filtering with applications to positioning, tracking and navigation.

E-mail: cheng.cheng@nwpu.edu.cn

**ZHANG Jiaolong** was born in 1988. He received his Ph.D. degree in weapon launch theory and technology from Northwestern Polytechnical University. Currently he is an associate researcher at the School of Astronautics, Northwestern Polytechnical University. His research interests include overall structure of aircraft, electric servo system, and micro-satellites.

E-mail: zhangjiaolong@nwpu.edu.cn